

ATTACC the Quadratic Bottleneck of Attention Layers

Sheng-Chun Kao¹, Suvinay Subramanian², Gaurav Agrawal² and Tushar Krishna¹

¹Georgia Institute of Technology

²Google

¹*skao6@gatech.edu, tushar@ece.gatech.edu*

² *{suvinay, chipguy}@google.com*

ABSTRACT

Attention mechanisms form the backbone of state-of-the-art machine learning models for a variety of tasks. Deploying them on deep neural network (DNN) accelerators, however, is prohibitively challenging especially under long sequences. Operators in attention layers exhibit limited reuse and quadratic growth in memory footprint, leading to severe memory-boundedness. This paper introduces a new attention-tailored dataflow, termed FLAT, which leverages operator fusion, loop-nest optimizations, and interleaved execution. It increases the effective memory bandwidth by efficiently utilizing the high-bandwidth, low-capacity on-chip buffer and thus achieves better run time and compute resource utilization. We term FLAT-compatible accelerators ATTACC. In our evaluation, ATTACC achieves 1.94x and 1.76x speedup and 49% and 42% of energy reduction comparing to state-of-the-art edge and cloud accelerators.

1. INTRODUCTION

Attention mechanisms have enabled state-of-the-art performance across a wide range of machine learning tasks—from natural language processing (NLP) [73], to object detection [12, 67, 90], image generation [13, 27, 53], and music synthesis [33, 34]—and are expected to serve as the foundation for a whole new generation of machine learning models in the coming years. At the same time, there has been increased interest in long-sequence tasks. For example, image generation (sequence length $N=12K$ [18, 21, 23]), paragraph summarization ($N=64K$ [44]), language modeling ($N=69K$ [57]), music processing ($N=1024K$ [21]), and more upcoming new applications. The development of benchmarks for long-sequence tasks [71] is testament to the importance and surging interest in the machine learning community for long-sequence attention-based models.

The run time and energy efficiency of attention layers, however, pose two key challenges: (1) quadratic complexity in compute and memory, and (2) limited reuse (§2). **Quadratic complexity** arises because the *attention matrix* computation and memory footprint of the corresponding tensors grow quadratically, $O(N^2)$, with the *sequence length* (N). This introduces a significant performance bottleneck, especially for models targeting longer sequence lengths ($>10K$) that are becoming increasingly prevalent [11, 44, 50]. **Limited reuse** arises because computation of the *attention matrix* involves activation-activation tensor operations. This is distinctly dif-

ferent from the convolution (CONVs) or fully connected (FCs) operators that involve activation-weight tensor operations. In activation-weight operations, the weights may be reused by multiple activations (e.g., by batching). By contrast, activation-activation operations require fetching unique sets of activations for each output element resulting in far lower reuse and correspondingly imposing a large memory bandwidth (BW) requirement¹. From our evaluation, a state-of-the-art datacenter-class accelerator with a BW of 400 GB/s can run a max sequence length of 4K before failing to maintain 80% compute utilization.

At the system level, dataflow optimization approaches, which orchestrate the data access and compute scheduling for better run time and energy efficiency, have demonstrated success in many CNNs, RNNs, and FC-based models. These include manually-optimized dataflows [1, 15, 39], and design-space exploration (DSE)-based methods [36, 40, 52]. However, these previous works often target individual operators with good reuse opportunities (CONV, GEMM, FC). They cannot solve the quadratic bottleneck in attention layers or the limited reuse problem of activation-activation operations. At the model level, techniques such as quantization and sparsity (via pruning, etc.) can improve efficiency for attention-based models [28, 32, 43, 60, 64, 77, 80, 87, 89]. These techniques, however, impact the model quality: they may require additional training, and/or changes to the model structure (e.g., larger, but sparse models). Techniques such as learned sparse attention (e.g., local-global attention) try to exploit empirically observed sparsity in the attention matrix [11, 18, 22, 44, 54, 55, 59, 65, 70]. Further, new mechanisms that address the fundamental quadratic complexity of attention while retaining its key insights, such as Linformer [78], low-rank matrix decomposition, and kernel methods are a subject of active research in the ML community [20, 21] (§7).

In this paper, We propose a new dataflow tailored for attention layers, called **F**used **L**ogit **A**ttention (FLAT). FLAT is motivated by the observation that the high BW requirement of attention layers on typical inference accelerators is actually from moving the inter-operator (intermediate) tensor back and forth between memory, and the problem exaggerates when dealing with $O(N^2)$ attention matrix. FLAT performs cross-operator (i) fusion and (ii) loop-nest optimizations (ordering and tiling) across the Logit and Attend operators within attention layers as they add the highest intermediate memory

¹In the paper, by BW we refer to the bandwidth to *off-chip memory* (DRAM/HBM), unless explicitly stated otherwise.

footprint; this enables memory-optimized interleaved execution of these operators. By appropriately sizing the cross-operator tile (i.e., intermediate tensor footprint) given a target accelerator, we are able to stage it completely within the limited on-chip buffer, completely eliminating off-chip accesses for the intermediate tensor. This allows FLAT to easily scale to large sequence lengths without becoming memory bound. FLAT targets inference accelerators and allows them to (i) effectively utilize the high-bandwidth, low-capacity on-chip memory resources, and (ii) achieve better utilization of computing resources, both of which we demonstrate via an accelerator instance called **ATTention ACCelerator** (ATTACC). FLAT is a generic dataflow optimization technique for attention-based models and is orthogonal to model-level techniques such as quantization/sparsity/attention matrix approximation described above; it can be applied on top of these techniques to further improve system efficiency without impacting model quality.

We make the following contributions:

- We characterize the tensor footprints for operators within attention layers, identifying the limitations posed by on-chip buffer sizes and memory bandwidth in running long sequence lengths (§3).
- We propose a new dataflow optimization approach, FLAT, applying specialized cross-operator loop-nest optimization to attention layers, which effectively utilizes low-capacity, high-bandwidth on-chip memory, and improves compute resources utilization, leading to better run time and energy-efficiency (§4).
- We identify minimum features for any SOTA accelerator to support FLAT, and call these FLAT-aware accelerators ATTACC (§5).
- We introduce a design space exploration (DSE) framework for running FLAT to optimize the performance metrics of interest (e.g., run time, energy) subject to varying resource constraints (e.g., area, on-chip memory capacity) for different attention-based models and usage scenarios (edge / cloud)(§5.3).
- ATTACC achieves 1.94x and 1.76x speedup and 49% and 42% of energy reduction in edge and cloud platform setting respectively, compared to an optimized baseline accelerator over a suite of attention-based models [23, 48, 49, 58, 73] (§6).

2. BACKGROUND ON ATTENTION

The attention mechanism [10] is emerging as a fundamental building block for several ML models and growing popular by the day. Attention-based models have demonstrated state-of-the-art performance across a wide range of tasks—from neural machine translation [56], to object detection [12, 67, 90], image generation [13, 27, 53], and music synthesis [33, 34], among many other applications [19]—often surpassing the performance of CNN-/RNN-based models.

2.1 Terminology for Attention-based Models

The most prevalent use of attention is in Transformer models [49, 68, 74]. Such models share similar architectures. In a top-down view (Figure 1), an attention-based **model** comprises multiple (often identically parameterized) attention

blocks². An attention block comprises multiple **layers**: an attention layer, a normalization layer, followed by multiple (typically two) fully connected layers. Finally, each layer comprises one or more **operations** or **operators**.

An attention layer comprises the following operators: i) Query (Q), Key (K), and Value (V) operators that perform a projection of the input tensor, ii) Logit (L) and Attend (A) operators that compute the attention matrix and attended output, iii) Output (O) operators that perform an output projection.

2.2 Computational Attributes

An attention layer comprises 6 operators: Q, K, V, L, A, and O. Figure 1(b-c) shows the computational graph of an attention layer involving these operators, the input/weight/output tensor sizes for each operator, and lists the notation for symbols. We categorize them into two: i) activation-weight operators (Q, K, V, O), which operate on activation tensors (from previous operators) and weight tensors (model parameters), and perform a GEMM computation as conventional fully connected operators (FCs), and ii) activation-activation operators (L, A), which operate on two activations from different previous operators and perform a GEMM computation.

To study the computational attributes of these operators, we characterize their **operational intensity** (*Op. Int.*). The operational intensity for an operator is defined as the number of arithmetic operations divided by the number of memory accesses. It captures the relative compute-/memory-boundedness of an operator. A lower operational intensity implies an operator has fewer opportunities for data reuse and is more BW-bounded. This directly impacts the design of the underlying accelerator and dataflow (§5, §3.2).

$$Op.Int. = \frac{Number\ of\ ops}{Number\ of\ memory\ accesses} \quad (1)$$

Activation-Weight operators (Q/K/V/O): For Q/K/V/O operators, following the notation in Figure 1(c), the number of operations is $O(BND^2)$. The number of memory access for the input (activations), weight (parameters), and output (activations) are $O(BND)$, $O(D^2)$, $O(BND)$, respectively. Therefore the operational intensity is $O(\frac{BND^2}{BND+D^2+BND})$. From the reciprocal, $1/Op.Int.$, $O(\frac{2}{D} + \frac{1}{BN})$, we see that increasing the batch size (B) can increase the operational intensity—the same weight value can be *reused* by multiple activations, leading to lower BW pressure. This is a typical technique used in activation-weight operators: it makes better use of the scarce memory bandwidth in accelerators and enables higher utilization of the provisioned compute FLOPs, leading to improved throughput.

Activation-Activation operators (L/A): For L/A operators, the number of operations is $O(BN^2D)$. The number of memory access for the two input-activations and the output-activations are $O(BND)$, $O(BND)$, $O(BN^2)$, respectively. Therefore the operational intensity is $O(\frac{BN^2D}{2BND+BN^2})$, and its reciprocal is $O(\frac{2}{N} + \frac{1}{D})$. Embedding size (D) is decided by the model, and sequence length (N) is decided by the application. For these operators, we are not able to simply leverage the

²Models may include a few other blocks: an embedding block with positional encoding and masking, and a few task-specific FC or CONV layers at the end.

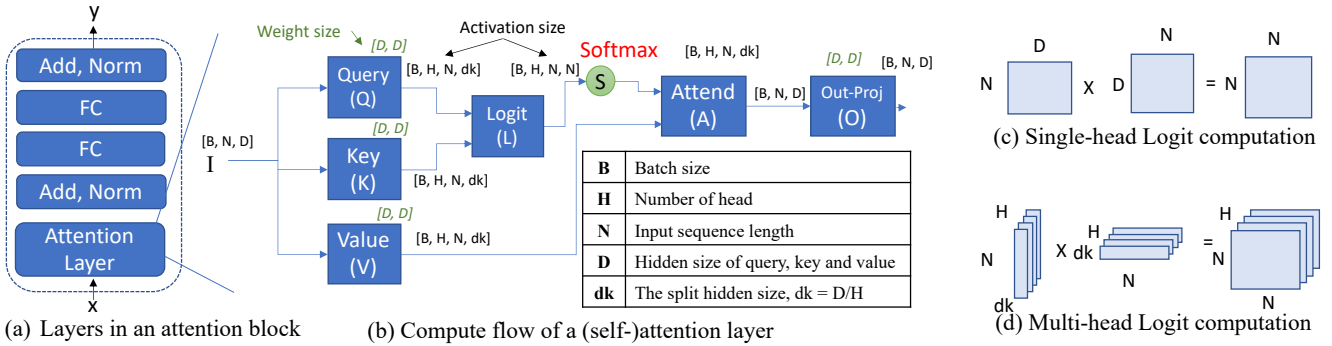


Figure 1: (a) Layers in an attention block. (b) Compute flow of an attention layer[†]. In (b), the blue box shows the operators; the green matrix notation shows the size of weight matrix; the black matrix notation shows the size of activation matrix; softmax is applied on output of Logit. (c) single-head and (d) multi-head computation in Logit.

[†]The Seq-length, N, in Query can be different from N in Key and Value in cross-attention.

batch size to increase the operational intensity. Instead, more involved approaches such as moving data on-chip need to be considered—this is discussed in more detail in §3.2.

Multi-head Attention An often-used variant of the attention mechanism is multi-head attention: it leads to higher accuracy in many tasks [73]. In multi-head attention, we split the output of the Q/K/V operator along a hidden dimension, reshaping it from size $[N, D]$ to $[H, N, dk]$, where $dk=N/H$. We then execute L operator to produce H tensors of size $[N, N]$, followed by the A operator, and finally aggregate the H tensors to size $[N, D]$ before executing O operator.

Note how the size of logit tensor grows by a factor H , while the number of computations remains unchanged compared to the baseline attention. This decreases the operational intensity for multi-head attention compared to the baseline. Specifically, for L/A operators, the number of operations is $O(BN^2D)$. The number of memory accesses for the two input-activations, and output-activations for L operator are $O(BND)$, $O(BND)$, $O(BHN^2)$ and for A operators are $O(BHN^2)$, $O(BND)$, $O(BND)$. Both L, A have an operational intensity of $O(\frac{BN^2D}{2BND+BHN^2})$, whose reciprocal is $O(\frac{2}{N} + \frac{H}{D})$. The lower operational intensity implies that multi-head attention is more memory-bound compared to the baseline attention. We discuss the implications of this on accelerator design, dataflow, and utilization in §3.

3. CHALLENGE: RUNNING ATTENTION LAYERS ON DNN ACCELERATORS

3.1 DNN Accelerators and Dataflow

DNN models are often executed on special hardware platforms or accelerators for improved run time and energy efficiency. A typical DNN accelerator (Figure 5) is composed of: (i) compute processing elements or PEs (each PE comprises a MAC unit and local scratchpad), (ii) on-chip memory that may be organized as single or multi-level hierarchies, and (iii) off-chip memory with higher capacity and lower bandwidth compared to on-chip memory. In this paper, we discuss our ideas in the context of a single-level on-chip memory hierarchy (i.e., the system we describe has a shared on-chip global scratchpad)—however, our ideas are applicable to a multi-level on-chip memory hierarchy as well.

Memory access is often the bottleneck [69] in executing

Table 1: The on-chip buffer size requirement to stage weights and activations on-chip. H: number of heads, N: sequence length, D: hidden dimension size.

Data bit width: 16bit	H	1	16	1	16	1	16
	N	512	512	2K	2K	14K	14K
	D	1024	1024	1024	1024	1024	1024
K/Q/V/O	Buf Req	4MB	4MB	10MB	19MB	62MB	62MB
L/A	Buf Req	2.5MB	10MB	16MB	142MB	474MB	6.6GB

DNN operators. Thus, DNN accelerators carefully *map* and *schedule* computations and associated data movement, exploiting opportunities for data reuse. This is referred to as *dataflow* and encompasses: (i) tiling (how tensors are sliced, stored and fetched across the memory hierarchy), (ii) compute order (order in which loop computations are performed), and (iii) parallelism (how compute is mapped across PEs in space).

Each tensor may be tiled (sliced) hierarchically typically (but not necessarily) corresponding to the on-chip memory hierarchy. *L1-tile* refers to the tile (slice) that is buffered within the PE array (local scratchpad). *L2-tile* comprises multiple L1-tiles: these are stored in the on-chip global scratchpad. Similarly, we can group multiple L2-tiles into an *L3-tile*: for an accelerator with a single-level on-chip memory hierarchy (i.e., a shared global scratchpad), L3-tiles can enable staging (pre-fetching) multiple L2-tiles and avoid being bound by off-chip memory bandwidth.

An individual operator in a DNN model may exercise different strategies for tiling, compute order, and parallelism. We refer to this as the *intra-operator dataflow*. For example, a CONV operator may be executed using a weight-stationary, [1], row-stationary [15] or output stationary [26] dataflow with specific tile sizes. Most standard dataflow optimization studies [40, 46, 52] focus on *intra-operator dataflow*.

One may also apply different strategies for tiling, compute order, and parallelism across multiple operators. We refer to this as *inter-operator dataflow*. Typically, DNN accelerators employ a compute order where one operator (e.g., CONV, FC) is executed at a time to completion. This sequential inter-operator dataflow is referred to as *baseline dataflow* in this paper. Note that each operator can be executed with its own intra-operator dataflow.

3.2 Attention v.s. FC v.s. CONV

In this section, we compare and contrast Attention opera-

tors (L, A) with other common DNN operators, CONV and FC, to illustrate the challenge in accelerating Attention layers. While all of these operators can be nominally cast as a GEMM, they have widely different computational attributes. Specifically, attention operators (L, A) exhibit (a) low reuse, and (b) large memory footprint (especially at long sequence lengths). These attributes preclude commonly used techniques in accelerators to improve performance as described below.

Low Reuse: CONV operators naturally exhibit high reuse with the filter being reused across several values (pixels) per input sample. This leads to high operational intensity, and thus CONV are a natural target for offloading to accelerators. The roofline plot in Figure 2(a) illustrates FC operators exhibit slightly lower reuse—each weight element is used once per input sample—and thus has lower operational intensity. A common technique to improve the operational intensity is to increase the batch size, which reuses a weight element across multiple input samples in a batch. This technique is widely used to improve the performance of FC operators. The roofline plot in Figure 2(b) illustrates how increasing the batch size can improve the performance for FC operators.

Attention operators (L, A) typically exhibit even lower operational intensity. These operators, however, are activation-activation GEMMs. Thus increasing the batch size does not increase the operational intensity and cannot improve the achievable performance. Figure 2(b)(d) illustrate this.

Large Memory Footprint: Another common technique to improve performance is to stage data on-chip and leverage the higher effective on-chip memory bandwidth. This raises the roofline ceiling as illustrated in Figure 2(c) and enables improved performance. However, this requires the live memory footprint to fit in the on-chip scratchpad capacity. For CONV, FC operators, the live memory footprint³ grows as $O(N)$, but for attention operators, it grows as $O(N^2)$.

Note that the above are fundamental limitations of the L, A operators, which cannot be overcome even with the most optimal *intra-operator* dataflow [15, 46, 52, 85] on any state-of-the-art accelerators.

4. FLAT DATAFLOW

We design a specialized dataflow strategy, Fused Logit Attention (FLAT), targeting the two memory bandwidth-bound operators in the attention layer, L and A. FLAT includes both intra-operator dataflow and a specialized inter-operator dataflow, that executes L and A in concert. The intra-operator dataflow utilizes any prior dataflows [15, 26, 46, 52].

4.1 Operator Fusion for Improved Utilization

The large live memory footprint in attention layer operators arises from the output-activation of L, which is also the input-activation of A. We refer to this tensor as the *intermediate tensor*, and it has size $O(BHN^2)$. We observe that, while the *entire* intermediate tensor can be inordinately large, slices (tiles) of this tensor are sufficient to generate slices (tiles) of the output of A.

FLAT leverages this observation and executes L and A in concert or in a *fused* manner. We limit the slice (tile) size of

³The on-chip buffer requirement to hold the data to avoid going to off-chip memory.

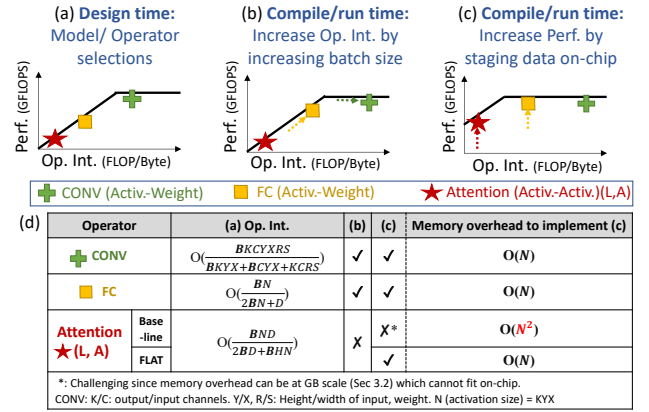


Figure 2: (a) Operation intensity (Op. Int.) and performance (Perf.) of operators, (b) batch-size impact on Perf., (c) staging data on-chip impact on Perf., and (d) the overhead to implement (c) and a summary of (a-c).

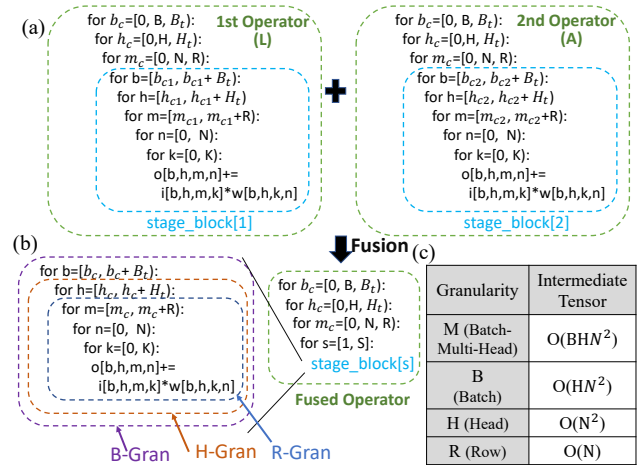


Figure 3: (a) Fused Operator Mechanism. (b) Choices of Granularity level. (c) Execution Granularity and Sizes of Intermediate Tensors. We omit the softmax function between the first and second operator for ease of depiction (§4.1 discusses details).

the intermediate tensor such that it can fit into the on-chip memory of a DNN accelerator: this reduced-size slice is used to generate the corresponding output slice of A. By executing portions of L and A computations entirely from the on-chip memory, FLAT enables higher effective memory bandwidth for these operators, which leads higher compute utilization and ultimately better performance.

While the generic idea of operator fusion is not new, it has not been explored in the context of attention layers. Further, attention layers introduce new challenges for operator fusion: (i) effectively handling large intermediate tensors that do not fit in on-chip memory, and (ii) respecting data dependencies across operators. We discuss how FLAT handles these below, and contrast against prior work in §7.

4.2 Cross-operator Fusion for Attention in FLAT

4.2.1 Compute and Loop Order

The loop nests for L and A are shown in Figure 4(a). To

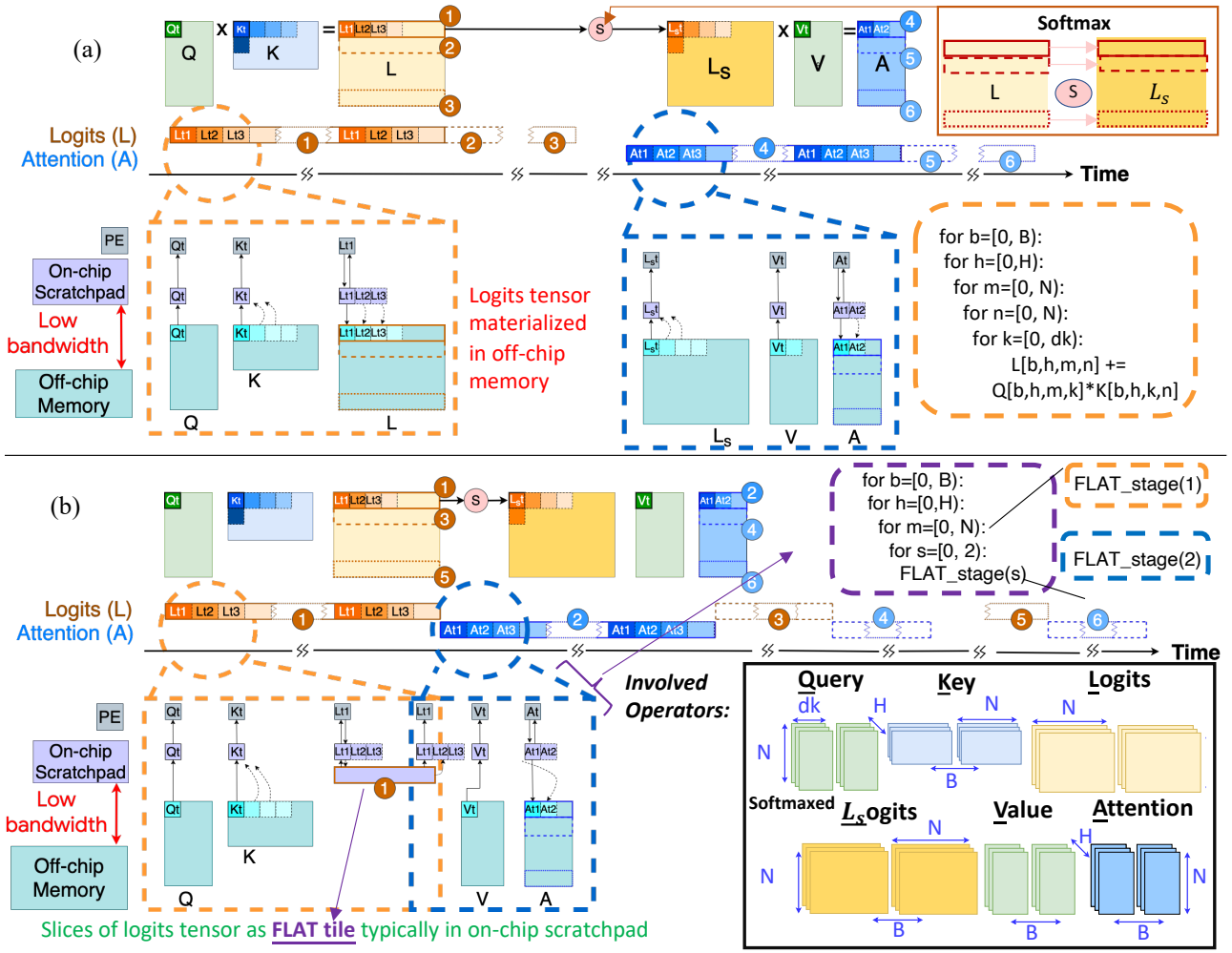


Figure 4: (a) Baseline and (b) FLAT dataflow. FLAT performs cross-operator fusion of L, A while respecting data dependencies introduced by softmax. FLAT-tile enables staging slices of the logits tensor in the on-chip scratchpad increasing effective memory bandwidth. This fused, interleaved execution of L, A yields higher compute utilization and improved performance.

fuse L and A, we divide the 5-level loop nest into two: cross-loop (outer-loop) and inner-loop, as shown in Figure 3. The cross-loops are shared across L and A. The inner-loops are unique for each operator. After fusion of two operators in the example in Figure 3 and Figure 4(b), the fused operator has two stages, which we run one after another (interleaved), and iterate through the shared cross-loop.

Cross-operator Data Dependency. The inner loops present a variety of tiling choices. However, these are constrained by a data-dependency between L and A: note that the output of L feeds into an activation function, which subsequently feeds into A. While activation functions such as ReLU operate element-wise on a tensor, the activation functions used in attention layers are more complex: specifically, a common choice is the softmax function [73] which requires a reduction along a specific dimension of the tensor before scaling individual elements. Arbitrary cross-loop fusion and tiling strategies as employed for CONV/FC layers [7, 82], will break this dependency and lead to incorrect results.

Basic execution unit: Row-granularity. The softmax reduction is along the key dimension (rows in L of Figure 4): this effectively captures the relative weight of each token in

the input sequence (query) against other tokens in the input (key). Therefore the basic softmax unit is a $[1, N]$ array, which requires a query of $[1, K]$ and a key of $[K, N]$. This is the finest granularity we require for the intermediate tensor slice, which will undergo a softmax operation between L and A operator (see Figure 4). We name this basic unit, row-granularity. We can choose to tile different numbers of rows (R) depending on the available buffer sizes. Larger R can enable greater reuse of the Key matrix, and hence higher data reuse while having larger live memory footprint. R becomes a hyper-parameter to explore in the design space.

4.2.2 Tiling

FLAT employs three levels of tiling: L1-tile, L2-tile (analogous to the baseline dataflow), and FLAT-tile. The FLAT-tile is an L3-tile for the fused-operator. In other words, FLAT computes FLAT-tile activations from L and feeds it directly to A⁴. FLAT-tiles, the blue box in Figure 3(a), in each stage essentially specify how many slices of the partial intermediate tensor are calculated in one pass of the fused-operator.

⁴In contrast, a L3-tile in the baseline computes L and A at the L3-tile granularity, but needs to run the full L operator before moving to A.

For example, the naive FLAT-tile, when sufficient on-chip buffer is available, is to have a FLAT-tile as large as the entire tensor, which makes the blue box the same size as the green box in Figure 3(a), which means pre-fetching entire tensor on-chip and compute the consecutive stages without going off-chip. In a buffer-limited situation, we want to explore small FLAT-tiles choices, discussed later.

FLAT-tiling and Execution Granularity In the 5-level for loop for the L, A operators, as shown in Figure 4(a), FLAT-tile needs to include at least the bottom two levels of for loop to keep the basic unit, row-granularity. This leaves us three hyper-parameters in FLAT-tile: number of rows (R), head tile size (H_t), and batch tile size (B_t). We refer to these as Row (R-Gran), Head (H-Gran), and Batch (B-Gran) execution granularity respectively. Further, for the most intuitive baseline of moving entire intermediate tensor on-chip is referred to as Batch-Multi-Head granularity (M-Gran).

L2, L1 Tiling. Since data dependency across L and A is captured by the FLAT-tile, there is no dependency constraint for the L2/L1 tiling strategy of each operator. Arbitrary L2, L1 tiling, captured by any prior dataflow [40, 52] can be specified.

Selectively Enabled FLAT-tile. A complete FLAT-tile includes one or more (typically two) input tensors, and output tensors. We can also selectively enable only a subset or all of them in FLAT-tile. Disabling parts of FLAT-tile will reduce live memory footprint. It, however, increases the risk of memory-BW-boundedness, since the disabled tensor follows the baseline dataflow which has higher BW requirements. We add the choice of enabling/disabling FLAT-tile for each tensor as separate hyper-parameters.

4.3 Walk-through Example

We show a walk-through example of executing L and A operator with FLAT dataflow using R-Gran in Figure 4(b). Based on the available on-chip buffer size, we could have different configurations of whether to enable FLAT-tile or not. In the L-A operator, there are 2^5 (Q, K, V, L/L_s, O) different enable/disable choices, and we show one of the configurations, only enabling L/L_s in Figure 4(b). The execution steps are as follows. We pre-fetch the FLAT-tile needed for L-A operators, two inputs of L and one inputs of A, and then start the computation. The two input L2-tile of L is fed into PE array and the output L2-tile of L is computed and stored back in on-chip buffer, which starts building up the output FLAT-tile of L. After output FLAT-tile of L is completed, they are sent to the special function unit, which compute softmax, and the softmaxed outputs are staged back in on-chip buffer. The softmaxed FLAT-tile becomes the input of A, and the output L2-tile of A get computed. Next, since we specify the output FLAT-tile of A to be disabled not leveraging FLAT-tile, whenever an output L2-tile of A is computed, it will directly send back to the off-chip memory. When all the output L2-tile of A are sent back, one iteration complete. Then, we iterate again according to the cross-loop specification.

4.4 Live Memory Footprint

Table 2 lists the required on-chip buffer size using FLAT. We derive the R-Gran value here (others follow a similar reasoning). Assuming all FLAT-tiles are enabled, L operator

Table 2: Buffer requirement for tiling granularity. M: batched Multi-head, B: Batch, H: Head, R: Row.

Granularity	M-Gran	B-Gran	H-Gran	R-Gran
Live Mem.	$O(8BDN + BHN^2)$	$O(8DN + HN^2)$	$O(8Ndk + N^2)$	$O(4Rdk + 4Ndk + RN)$
Footprint				

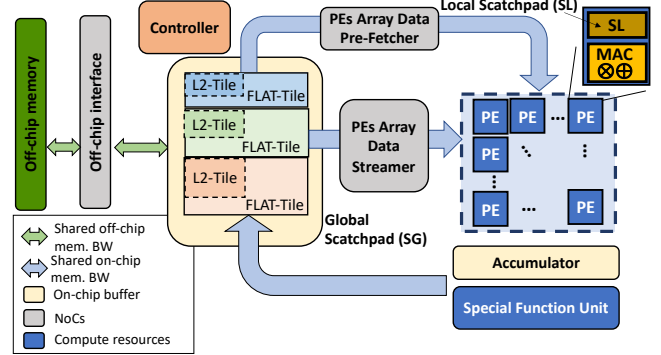


Figure 5: Architecture of Baseline and ATTACC accelerator. Baseline performs sequential execution of all operators, while ATTACC supports interleaved execution of L-A operators by streaming FLAT-tiles through SG.

consumes $(Rdk + Ndk) \times 2$ (2 to account for double buffering, see §5), A consumes $(Ndk + Rdk) \times 2$, and RN for the shared intermediate tensor (no double buffering since it does not interact with off-chip memory). Thus, the live memory footprint only grows as $O(N)$ complexity with FLAT at R-gran.

4.5 FLAT on Other Operators

Decision of Number of Fused Operator in Attention Layer. We choose to fuse L and A but leaving others (K, Q, V, O) un-fused. Note that the more operators we fuse, the more data we need to stage partially on-chip. While one of the main goals of operator fusion is to reduce the memory footprint of the intermediate tensors, the intermediate tensors between K-L, A-O, etc., do not exhibit the quadratic growth problem. Therefore, the benefit of fusing other operator become limited and can otherwise deteriorate the performance owing to larger memory footprint.

Running Non-fused Operator with FLAT. FLAT can also represent the baseline single operator dataflow by degrading the cross-operator tiling to a single-operator tiling. To be specific, we disable fuse operations. Expressing other normal non-fused operators (K/Q/V/O/FC) with FLAT still has the benefit of adding the exploration of different granularity (H-gran, B-gran, M-gran) and the enabling/disabling of L3-tile choices, while many baseline dataflows did not leverage tiling at this hierarchy level. It would potentially allow more interesting design choices and lead to dataflow with better performance.

5. ATTACC ARCHITECTURE AND DSE

We describe the minimum set of features needed in an accelerator to be FLAT-compatible. We call such an accelerator as ATTACC (ATTention ACCelerator).

5.1 Features of ATTACC

(1) **Soft-partitioned double-buffered scratchpad.** The global scratchpad inside the accelerator needs to be fully

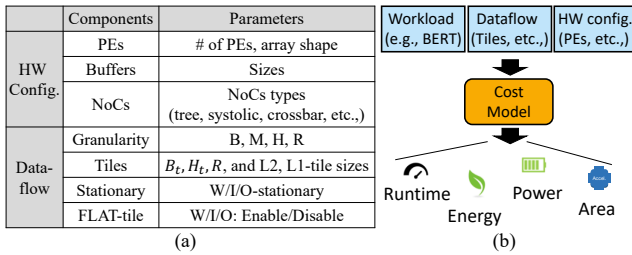


Figure 6: (a) The parameter of cost models. (b) The cost model of ATTACC with FLAT dataflow.

flexible (i.e., addressable) to partition for two hierarchy levels of tile sizes during execution of the fused L-A operators: L2-tile and FLAT-tile, for input and output tensors. Many datacenter-class accelerators already employ fully programmable scratchpads [8, 38, 63] and should be able to create the soft-partition across FLAT-tiles and L2-tiles without any area overhead.

(2) Interleaved Execution of fused-operator. The fused-operator can be executed either in an interleaved manner or in a pipelined manner. In interleaved execution (*aka* temporal pipelined), all PEs compute the FLAT-tile of L and feed it back to the PE array (after a softmax) to now compute A, followed by the next FLAT-tile of L, and so on. In (spatially) pipelined execution, half the PEs can compute L and feed the output to the rest of the half running A. We found interleaving with double buffering to be a better implementation choice. First, interleaved execution requires minimal changes to the controller fetching tiles from SG while pipelining requires splitting the PE array, adding area overhead. Second, the pipelined array incurs fill and drain latencies. Third, the pipelined array becomes inefficient during the execution of non-fused operators. Fourth, interleaved execution ameliorates the off-chip memory bandwidth requirements of double buffering. When executing fused L-A operator, the *warm-up buffer* of stage-L can be fetched across the duration of two stages: when the *active buffer* of stage-L and the *active buffer* of stage-A are being worked on. The pipelined execution (and baseline), however, can only leverage one stage, viz., when that operator’s active buffer is being worked on.

5.2 Implementation of ATTACC

In this work, we implement the ATTACC features over a spatial DNN accelerator shown in Figure 5⁵. It comprises of a PE array, a global scratchpad (SG) (*aka* on-chip buffer in this paper) and special function unit (SFU) for non-linear activations, reductions, and softmax. Inside each PE, there is a MAC and a local scratchpad (SL). Depending on the intra-operator dataflow, L2 tiles for one of the operands is pre-fetched into the PE array and held stationary, while the other operand is streamed in.

5.3 DSE methodology

We developed a detailed analytical cost model for estimating the performance and energy for both a baseline accelerator and ATTACC running FLAT, as shown in Figure 6. The cost model was built similar to some previous works such as Timeloop [52], MAESTRO [3], and SCALE-Sim [61].

⁵Note that FLAT can be implemented and run over a GPU as well, though not the focus of this work.

However, unlike these models [3, 52, 61] that only leverage intra-operator dataflow and cannot explore the design space enabled by FLAT, our cost-model can model both inter- and intra-operator dataflows and the mix of them, supports all the techniques involved in FLAT, and is backward compatible to MAESTRO [3] (which in turn is RTL-validated [46]).

5.3.1 Performance Model

Compute Model. We model the compute array as a collection of PEs with configurable bandwidth from/to the SG buffers. The compute array can support any intra-operator dataflow (weight/input/output stationary) which is modeled by appropriately setting which tiles are stationary and which are streamed in. We also model different choices for data distribution and reduction NoCs (systolic, tree, crossbar) which trade-off bandwidth and distribution/collection time [46, 47]. This allows us to model both systolic arrays (e.g., TPU [39]) to more flexible spatial arrays (e.g., Eyeriss_v2 [16] and MAERI [47]), which form our baseline accelerators. We model the overhead for switching tiles (filling and draining of the array) to reflect the cold start and tailing effect. We also account for the runtime for SoftMax as it comes between the L and A operators and in our critical path.

Buffer Model. The SL inside each PE is a scratchpad for holding three elements: input, weight, and output of L1-tile. The SG is an on-chip buffer for holding L2-tile or FLAT-tile. We also model different enabling/disabling choices for FLAT-tile. While the live memory footprint is larger than the SG buffer, we model the data to be partially fetched on-chip and partially fetched off-chip. Also, while input/weight/output occupies the memory, the space for the partial sum is also often an unignorable overhead, which we also precisely capture.

Memory BW Model. As shown in Figure 5, there are multiple units that could interact with on-chip and off-chip memory. However, the memory BW is limited. Therefore, we model the on-chip and off-chip memory as a limited shared HW resource. That is, when multiple units are requesting data from the memory and the number of data requested exceeded the memory BW, it incurs larger memory access overhead. We model detailed data transfer across the memory hierarchy. In our cost model, we track both foreground (active stage) and background (warm-up stage) tasks, and all of them shared the limited on-chip/ off-chip BW.

5.3.2 Energy Model

Based on activity counts generated by the performance model, we leverage Accellergy [84] to estimate the energy for compute, on-chip memory and off-chip memory accesses for both the baseline and ATTACC accelerators running several design-points of the dataflows. Note that FLAT does not change the total computations or the total buffer accesses to SG; what it changes is the number of off-chip accesses (which are orders of magnitude more expensive in energy than on-chip [15, 69]).

5.3.3 Dataflow and Tile size Exploration

Our cost model enables design-space exploration of all the hyper-parameters in FLAT, which are listed in Figure 6(a). Each unique combination of the hyper-parameters forms a

(a) Platform	# of PEs	On-chip Buffers	On-chip BW	Off-chip BW
Edge	32x32	512KB	1TB/sec	50GB/sec
Cloud	256x256	32MB	8TB/sec	400GB/sec

(b) Dataflow Configuration	Enable L3/FLAT-tile	Granularity	L, A operator	Hyper-parameter Search (DSE)
Base	No	M	Seq	No
Base-X	Yes	M, B, H	Seq	No
Base-opt	Yes	by DSE	Seq	Yes
FLAT-X	Yes	M, B, H	Fused	No
FLAT-Rx	Yes	R (# Row=Rx)	Fused	No
FLAT-opt	Yes	by DSE	Fused	Yes

(c) Accelerator Configuration	Dataflow	Flexible dataflow support	Granularity
BaseAccel	Base	No	M
FlexAccel-M	Base-opt (M-Gran only)	Yes	M
FlexAccel	Base-opt	Yes	by DSE
ATTACC-M	FLAT-opt (M-Gran only)	Yes	M
ATTACC-Rx	FLAT-opt(Rx-Gran only)	Yes	R (# Row=Rx)
ATTACC	FLAT-opt	Yes	by DSE

FlexAccel/ATTACC-X: Accel with flexible dataflow but fixed X-granularity.

Figure 7: (a) The HW resource configuration of cloud and edge accelerators in the evaluation sections. The configurations of the comparing (b) dataflows and (c) accelerators. FlexAccel represents SOTA accelerators with SOTA frameworks. ATTACC represents SOTA accelerators with **FLAT-enhanced** SOTA frameworks.

unique design point as we discuss in §6.1. We use exhaustive search to find the optimum point under the user-specified objective, e.g., best run time.

6. EVALUATIONS

6.1 Evaluation Setting

Workloads. We explore different attention-based models, including BERT (BERT-base [73]), FlauBERT [49], XLM (xlm-mlm-en [48]), TransformerXL [23], and T5 (T5-small [58]). We explore different sequences length on these models from N=512 to N=64K [11, 44] and the future-proofing size of N=256K. We run all the models with batch size of 64.

Performance Metric. We use compute resource utilization (Util) as the primary performance metric, defined as:

$$Util = \frac{Runtime_{ideal}}{Runtime_{actual}}$$

where $Runtime_{ideal}$ is the ideal run time of the target operations given fully utilized PEs, and $Runtime_{actual}$ is the run time of the operations considering all the HW overhead, including memory bandwidth, memory sizes, on-chip data movement (distribution and reduction). Our DSE framework allows using energy or area as metrics to optimize for as well.

Platform Resources. Based on previously proposed cloud [4, 38, 72] and edge [2, 16, 86] accelerators, we select the amount of hardware resources for cloud and edge accelerator settings as described in Figure 7(a), and for both of them, we run the accelerator at 1GHz.

Baseline Dataflow. We compare FLAT with three baseline dataflows, as shown in Figure 7(b). Base reflects the dataflow strategy used in many DNN accelerators [1, 2, 26], which does not leverage cross-operator tiling and hence does not have a L3-tile (§3.1) in the design space. Base-X is an augmented version of Base, which considers L3-tile with X

granularity (where X=M/B/H). Base-opt is the optimal non-fused dataflow that can be found via dataflow DSE (§5.3.3). Recall that the baseline dataflow does not do cross-operator fusion. The baselines with L3-tiles prefetch and compute L and A at X granularity, but the dataflow iterates through the entire L tensor before starting A.

FLAT dataflow. We also formulate different versions of FLAT for comparisons. FLAT-X and FLAT-Rx are FLAT with X-Gran and R-Gran (with Rx rows). FLAT-opt is the optimal dataflow found by DSE in FLAT design space.

Baseline Accelerator. We compare with three categories of baseline accelerators, as shown in Figure 7(c). (i) BaseAccel is a conventional DNN accelerator running a fixed Base dataflow [1, 17, 26]. (ii) FlexAccel is an accelerator with full flexibility (e.g., MAERI [47]) for running any intra-operator dataflow (i.e., Base-opts) found via dataflow DSE. (iii) FlexAccel-M represents flexible accelerators with support for L3-tiling at M-Gran; but finer-grained L3-tiles (like FLAT) cannot be leveraged. Many baseline accelerators with fully programmable scratchpads can fall into this category [8, 38, 63].

ATTACC accelerator. Following the same naming scheme as baseline accelerators, ATTACC is a fully-flexible accelerator which supports FLAT dataflow with an optimal sized FLAT-tile. For comparisons, we also show two fixed FLAT-tile granularity versions: ATTACC-M and ATTACC-Rx, as shown in Figure 7(c). In the evaluations, we make sure SFU (Figure 5) has enough FLOPs to not bottleneck the compute flow for all variants of baseline/ATTACC accelerators.

Comparing Environment Setup. We use the detailed cost model described in §5.3 to model the performance of different dataflows and accelerators with different levels of platform resources: Cloud and Edge (Figure 7(a)). We set the bit-width of the model to be 16-bits throughout our evaluation. The performance of an accelerator depends on dataflow, HW resources, and workloads. Given these three, the cost model outputs the performance report of the accelerator, including run time, compute utilization, and energy consumption.

6.2 Utilization

6.2.1 Edge Platform Resources

Recall the definition of Util from §6.1. Lower Util implies higher run time and lower throughput. As shown in Figure 8(a)-L-A-Len512, the Base (sequential inter-operator) dataflow has around 0.2 Util when the buffer size is small and has a peak Util of 0.6, when adequate buffer is provided. It demonstrates the challenge for many existing accelerators when running attention-based models, *viz.*, low compute utilization (low Util).

Base-M is dataflow with a L3-tile operating at the granularity of the entire intermediate tensor (i.e., multi-batch-head). By staging data on-chip, Base-M can potentially increase the Util, since ideally the interfacing memory BW is much higher than Base. However, when the on-chip buffer size is not adequate to house the tensors, the accelerator needs to fetch partial tensors from on-chip and the rest from off-chip. It introduces one extra pass of memory access for each of the data compared to Base, and thus has lower performance when on-chip buffer is limited. However, when the on-chip buffer is adequate, Base-M exceeds the performance of Base,

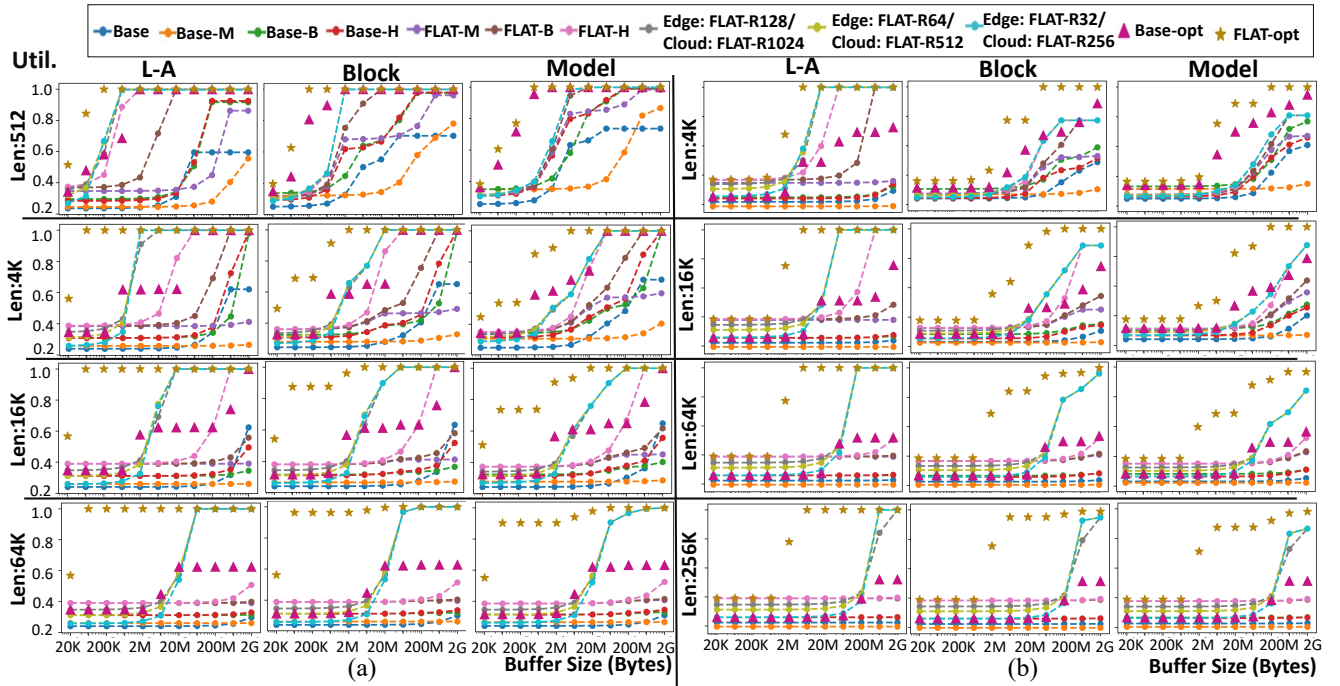


Figure 8: Comparisons of compute utilization across different platforms, models and sequence lengths. We sweep the available on-chip buffer from size 20KB to 2GB and show the performance under sequence length of 512 words to 256K words. We list three level of performance analysis, L-A: focusing on performance difference at the L, A operators; Block: consider all operators in the attention block; and Model: a model-wise performance. (a) Running BERT under edge platform resources. (b) Running XLM under cloud platform resources.

as the trend shown in Figure 8(a)-L-A-Len512. Base-B and Base-H are two variants with smaller granularity. They have smaller live memory footprint for on-chip buffer, whose Util can approach near 0.92 when the on-chip buffer size is large. FLAT-M, FLAT-B, FLAT-H, and FLAT-Rx show that FLAT can effectively increase the cap Util compared to their Base counterparts. The finer-grained dataflow, FLAT-Rx, which is enabled by FLAT (but cannot be leveraged by Base), can approach near 1.0 cap performance and requires much smaller on-chip buffer to reach the cap performance, which shows the effectiveness of the fine-grained execution that FLAT provides.

To show the potential performance in the full design space of Base-X and FLAT-X, we run DSE for both of them and get their optimal points, Base-opt and FLAT-opt. FLAT-opt always outperforms Base-opt, as shown in Figure 8(a)-L-A-Len512 and other sub-plots in Figure 8.

We show similar comparisons for different sequence lengths in rows 2–4 of Figure 8(a). As the sequence length grows, the live memory footprint of on-chip buffer increases quickly ($O(N^2)$) as discussed in §3.2. Thus the larger granularity options can only reach low Util under limited on-chip buffer (20KB - 2GB) in the experiments. For L-A in Figure 8(a), FLAT-Rx becomes the only dataflow that can approach their cap Util region when the sequence is longer than 64K. It is worth noting that the most optimized baseline dataflow, Base-opt, still has low performance because it does not have the ability to leverage cross-operator and finer-grained R-Gran.

Note that we consider the operator fusion for only L and A operators (based on our observation in §4.5) and keep the other operators non-fused. In Figure 8(a)-Block/Model-

Len512, we observe how the effect of L, A operators are diluted when more operators are considered. Note that other operators are mostly FC/GEMM where typical single (intra-)operator dataflow is sufficient to reach high Util, and hence most of the baseline show higher performance in Block-wise and Model-wise performance. However, L and A become BW intensive when the sequence lengths are large, where the performance of L and A operator becomes dominant quickly. In Figure 8(a), we can see that FLAT can enable high Util, close to 1.0, even with large sequence length, across the hierarchy of L-A operator level, block level, and model level.

6.2.2 Cloud Platform Resources

In Figure 8(b), we show the evaluation under cloud platform resources with sequence lengths ranging from 4K to 256K. For the FLAT-Rx configuration, we pick larger size of Rx, since we have larger a PEs array to leverage (Figure 7(a)). When the sequence length is larger than 16K, we observe that most Base-X has Util lower than 0.4 in L-A cases. Base-opt can find solution with near 0.8 Util when the buffer size is large and sequence length is smaller than 16K. However, it fails to find good solution when the sequence length further increases. A similar trend can also be observed at hierarchy level of block and model.

6.3 Energy Consumption

For each of the data point in Figure 8, we show their energy consumption in Figure 9. It is worth noting that high Util in Figure 8 does not directly imply good energy performance in Figure 9; however they are highly correlated. Data points with high Util usually have better memory access pattern (less off-chip memory access and more reuse) and thus cost less

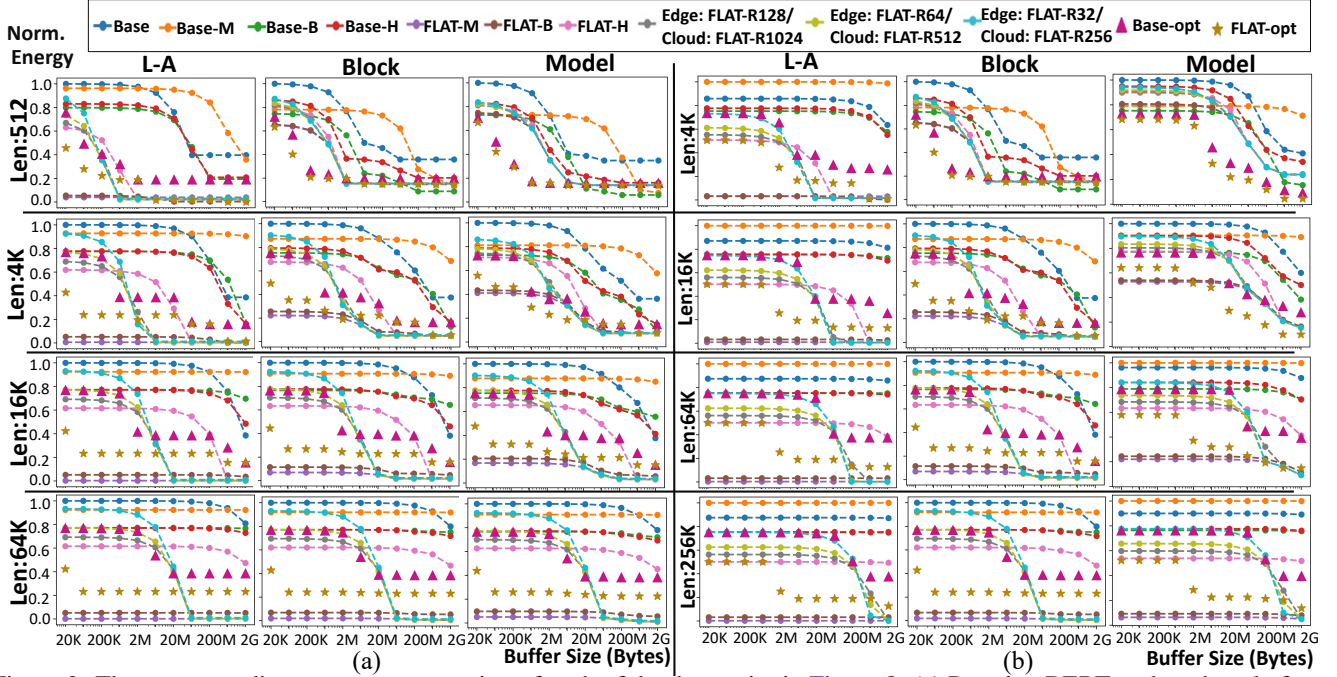


Figure 9: The corresponding energy consumption of each of the data-point in Figure 8. (a) Running BERT under edge platform resources. (b) Running XLM under cloud platform resources. The energy numbers are normalized by the largest energy number in each sub-plot.

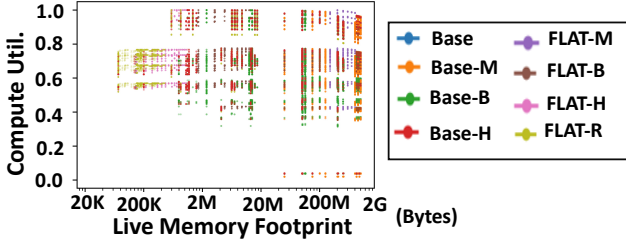


Figure 10: The design space of FLAT when running BERT with sequence length of 512 under edge platform resources.

memory access energy, which is usually the most dominant part in the energy consumption of accelerators. In Figure 9, we observe FLAT-X and FLAT-opt, generally have lower energy consumption than Base-X and Base-opt. One important factor for this advantage is the saved off-chip memory accesses from operator fusion, as discussed in Figure 4.

In Figure 9(a)-L-A-Len512, we observe that some data points of FLAT-opt have larger energy consumption than the one of FLAT-X and FLAT-Rx. Since FLAT-opts are optimal points maximizing Util, which could take larger energy. This observation can also be found in Base-X and Base-opt cases, e.g., Base-B and Base-opt in Figure 9(a)-Block-Len512. However, the objective target in the DSE is flexible, which can also be set as best energy. It would make FLAT-opt and Base-opt reach the optimal energy point in their own design spaces.

6.4 Dataflow DSE

We show the entire design-space for FLAT dataflow in Figure 10. The top-left corner means reaching high utilization with the least live memory footprint. For each dataflow, there are many hyper-parameters that can be tuned which becomes one unique data point in the design space graph in

Figure 10. The optimal points are picked based on the objective. For example, in our study, the objective is maximum Util. Different objective could be used such as the best Util per memory footprint, leading to points in top-left corner, or the least memory footprint, leading to points in the left-most region.

6.5 Comparisons of Accelerators

6.5.1 Accelerator Performance

We formulate two versions of ATTACC, ATTACC-edge and ATTACC-cloud, with different HW resources as listed in Figure 7(a). Two different baseline accelerators BaseAccel and FlexAccel (in Figure 7(c)) are compared, and both are formulated with two type of resource budgets: cloud and edge. We categorize the operators in attention-based models into three category: (i) L-A operators, (ii) Projection operators, other operators in attention layer (K/Q/V/O), and (iii) FCs, the two FC operators outside the attention layer. These were shown earlier in Figure 1. We also plot the non-stall-latency, the ideal run time given the compute resources, as shown in Figure 11. FlexAccel and ATTACC share the same performance for Projections and FCs. It is because in ATTACC, both Projections and FCs are treated as non-fused operators and hence the design space for them are the same as the one in FlexAccel. In Figure 11(a), when the sequence length is 512, ATTACC and FlexAccel can both reach near optimal performance. However, when the sequence length increases, the performance difference becomes more significant. In the cloud cases (Figure 11(b)), the performance difference exaggerates, and the run time of L-A operators starts to dominate the run time performance.

Comparisons across variants of models. We compare the performance difference across multiple models. As shown in Figure 12(a), comparing to FlexAccel-M and FlexAccel,

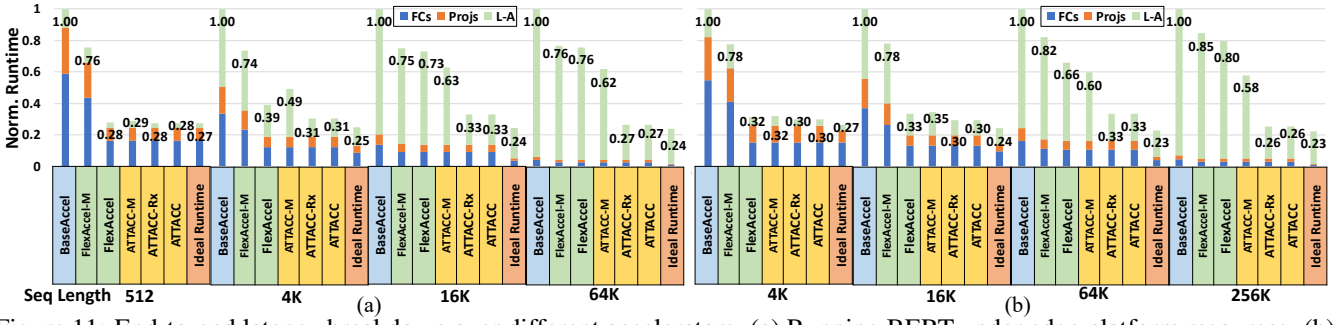


Figure 11: End-to-end latency breakdown over different accelerators. (a) Running BERT under edge platform resources. (b) Running XLM under cloud platform resources.

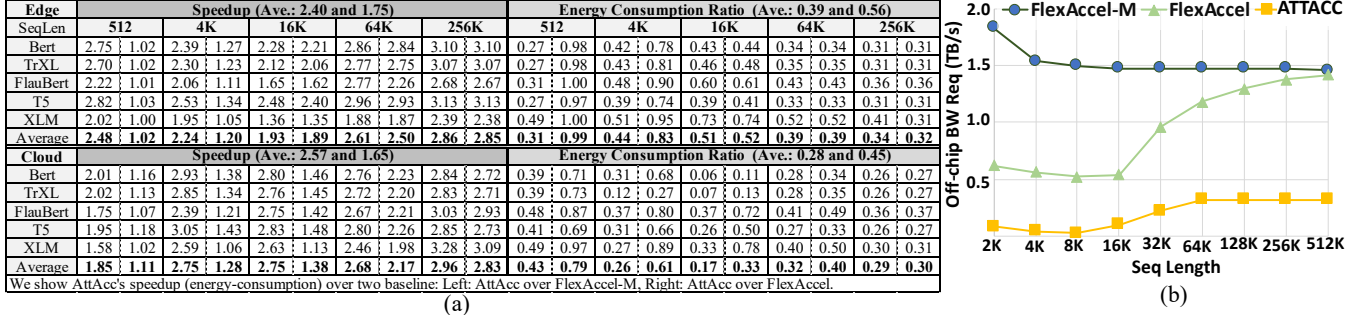


Figure 12: (a) The speedup and energy-consumption ratio of ATTACC over FlexAccel-X and ATTACC over FlexAccel on different models and resources with the respect of model-wise performance. (b) The required BW to reach utilization rate higher than 0.95 in the most BW-intensive L-A operator in when running XLM under cloud platform resources.

ATTACC achieves **2.52x** and **1.94x** speedup in edge cases and **2.60x** and **1.76x** speedup in cloud cases, while reducing the energy by **60%** and **49%** in edge cases and **69%** and **42%** in cloud cases, owing to its better memory access and reuse pattern.

6.5.2 BW Requirements

Effectively using the limited off-chip BW is an important factor for the scalability of the HW accelerator in the system because DNN operation is often memory-bound and the off-chip BW is often shared across different components in the system. In Figure 12(b), we show the off-chip BW requirement to peak the Util at 0.95 at the most BW-bounded L-A operator. As discussed in §2.2, the operation intensity increases with the sequence length and hence can reach Util of 0.95 earlier at lower off-chip BW (before around 4K-8K of Figure 12(b)). However, the live memory footprint increases with the sequence length. When the available on-chip buffer, 32MB in this experiment, is not sufficient to house the instantiated on-chip data, data will be partially fetched from off-chip, thus imposing higher off-chip BW requirement (after around 4K-8K of Figure 12(b)). Overall, ATTACC reduces the off-chip BW requirement by **88%** and **82%** against FlexAccel-M and FlexAccel on average. Similarly, when evaluated under the edge scenario running BERT, ATTACC achieves **76%** and **71%** reduction in off-chip BW requirement.

7. RELATED WORKS

Dataflow/ Mapping Approaches. Many recent DNN HW dataflow works focus on the CONV [1, 15, 24, 26, 30, 31, 36, 40, 51, 52, 63, 66, 75, 76, 85, 88] or GEMM [39, 81] accelerators.

design space, and use single operator dataflow, which can all be represented with L2-tile of FLAT. Some recent work also considers cross-operator dataflow [7, 82], targeting CNNs and leveraging pipeline execution. This work targets attention-based models and leverages interleaved execution, while respecting data dependencies. Andrei et al. [35] studied operation fusion in Transformer, however, in a coarse-grained fashion and without tiling and interleaving technique used in FLAT.

Model-level Approaches. At the model level, techniques such as quantization [43, 64, 87, 89], pruning [32, 60, 77, 80], and distillation [37, 62, 68, 79] are used for compressing attention-based models. Another line of research is to make fundamental change on the attention mechanism to reduce compute and memory complexity, including techniques such as local/global attention [11, 18, 54, 55, 65], learned sparsity [22, 44, 59, 70] low rank and kernel methods [20, 21, 41, 78], and others [11, 23, 57]. These techniques are orthogonal to the ideas developed in this paper. FLAT can also be leveraged in association with these techniques when deployed on DNN accelerators to further improve run time/energy performance.

Compiler Optimization. Fusion is a classic compiler technique widely employed in HPC [6, 25, 29, 42, 83] and ML compilers [5, 9, 14, 45]. However, ML compilers employ fusion in a limited fashion—they typically fuse matrix operators (FC, CONV) with element-wise ops (like ReLU). Further, they mostly consider only intra-operator tiling/unrolling/flattening. This work applies fusion across multiple matrix operators while respecting data dependencies of intraveneing operations, and incorporates both intra- and inter- operator tiling.

8. CONCLUSION

Running attention-based models with long sequences is challenging because of limited reuse and quadratic growth of live memory footprint. FLAT employs cross-operator fusion, loop-nest optimization, and interleaved execution. FLAT enables high compute utilization and reduced off-chip bandwidth requirements while scaling to long sequence lengths. FLAT is a new tool in a hardware architect's toolbox—it changes the design space and choices when designing an accelerator. Much like CONV-accelerators for vision, for accelerators tailored to attention (useful for several NLP-based tasks) designers can now budget a much smaller on-chip buffer. FLAT changes how available area (energy) is provisioned and balanced across compute/memory.

REFERENCES

- [1] "Nvidia deep learning accelerator," <http://nvidia.org>, 2017.
- [2] "Coral ai," <https://coral.ai/>, 2020.
- [3] "Maestro: An open-source infrastructure for modeling dataflows within deep learning accelerators," <http://maestro.ece.gatech.edu/>, 2020.
- [4] "Nvidia ampere gpu architecture tuning guide," https://docs.nvidia.com/cuda/pdf/Ampere_Tuning_Guide.pdf, 2021.
- [5] "Tensorflow xla," <https://www.tensorflow.org/xla>, 2021.
- [6] R. Allen and K. Kennedy, "Vector register allocation," *IEEE Computer Architecture Letters*, vol. 41, no. 10, pp. 1290–1317, 1992.
- [7] M. Alwani, H. Chen, M. Ferdman, and P. Milder, "Fused-layer cnn accelerators," in *2016 49th Annual IEEE/ACM International Symposium on Microarchitecture (MICRO)*. IEEE, 2016, pp. 1–12.
- [8] E. Baek, D. Kwon, and J. Kim, "A multi-neural network acceleration architecture," in *2020 ACM/IEEE 47th Annual International Symposium on Computer Architecture (ISCA)*. IEEE, 2020, pp. 940–953.
- [9] R. Baghdadi, J. Ray, M. B. Romdhane, E. Del Sozzo, A. Akkas, Y. Zhang, P. Suriana, S. Kamil, and S. Amarasinghe, "Tiramisu: A polyhedral compiler for expressing fast and portable code," in *2019 IEEE/ACM International Symposium on Code Generation and Optimization (CGO)*. IEEE, 2019, pp. 193–205.
- [10] D. Bahdanau, K. Cho, and Y. Bengio, "Neural machine translation by jointly learning to align and translate," *arXiv preprint arXiv:1409.0473*, 2014.
- [11] I. Beltagy, M. E. Peters, and A. Cohan, "Longformer: The long-document transformer," *arXiv preprint arXiv:2004.05150*, 2020.
- [12] P. Bhattacharyya, C. Huang, and K. Czarnecki, "Self-attention based context-aware 3d object detection," *arXiv preprint arXiv:2101.02672*, 2021.
- [13] M. Chen, A. Radford, R. Child, J. Wu, H. Jun, D. Luan, and I. Sutskever, "Generative pretraining from pixels," in *International Conference on Machine Learning*. PMLR, 2020, pp. 1691–1703.
- [14] T. Chen, L. Zheng, E. Yan, Z. Jiang, T. Moreau, L. Ceze, C. Guestrin, and A. Krishnamurthy, "Learning to optimize tensor programs," in *Advances in Neural Information Processing Systems*, 2018, pp. 3389–3400.
- [15] Y.-H. Chen *et al.*, "Eyeriss: An energy-efficient reconfigurable accelerator for deep convolutional neural networks," *JSSC*, vol. 52, no. 1, pp. 127–138, 2016.
- [16] Y.-H. Chen, T.-J. Yang, J. Emer, and V. Sze, "Eyeriss v2: A flexible accelerator for emerging deep neural networks on mobile devices," *IEEE Journal on Emerging and Selected Topics in Circuits and Systems*, vol. 9, no. 2, pp. 292–308, 2019.
- [17] Chen, Yu-Hsin and Krishna, Tushar and Emer, Joel and Sze, Vivienne, "Eyeriss: An Energy-Efficient Reconfigurable Accelerator for Deep Convolutional Neural Networks," in *IEEE International Solid-State Circuits Conference, ISSCC 2016, Digest of Technical Papers*, 2016, pp. 262–263.
- [18] R. Child, S. Gray, A. Radford, and I. Sutskever, "Generating long sequences with sparse transformers," *arXiv preprint arXiv:1904.10509*, 2019.
- [19] K. Cho, A. Courville, and Y. Bengio, "Describing multimedia content using attention-based encoder-decoder networks," *IEEE Transactions on Multimedia*, vol. 17, no. 11, pp. 1875–1886, 2015.
- [20] K. Choromanski, V. Likhoshesterov, D. Dohan, X. Song, J. Davis, T. Sarlos, D. Belanger, L. Colwell, and A. Weller, "Masked language modeling for proteins via linearly scalable long-context transformers," *arXiv preprint arXiv:2006.03555*, 2020.
- [21] K. Choromanski, V. Likhoshesterov, D. Dohan, X. Song, A. Kane, T. Sarlos, P. Hawkins, J. Davis, A. Mohiuddin, L. Kaiser *et al.*, "Rethinking attention with performers," *arXiv preprint arXiv:2009.14794*, 2020.
- [22] G. M. Correia, V. Niculae, and A. F. Martins, "Adaptively sparse transformers," *arXiv preprint arXiv:1909.00015*, 2019.
- [23] Z. Dai, Z. Yang, Y. Yang, J. Carbonell, Q. V. Le, and R. Salakhutdinov, "Transformer-xl: Attentive language models beyond a fixed-length context," *arXiv preprint arXiv:1901.02860*, 2019.
- [24] S. Dave, Y. Kim, S. Avancha, K. Lee, and A. Shrivastava, "Dmazerunner: Executing perfectly nested loops on dataflow accelerators," *ACM Transactions on Embedded Computing Systems (TECS)*, vol. 18, no. 5s, pp. 1–27, 2019.
- [25] C. Ding and K. Kennedy, "Improving effective bandwidth through compiler enhancement of global cache reuse," *Journal of Parallel and Distributed Computing*, vol. 64, no. 1, pp. 108–134, 2004.
- [26] Z. Du, R. Fasthuber, T. Chen, P. Ienne, L. Li, T. Luo, X. Feng, Y. Chen, and O. Temam, "Shidiannao: Shifting vision processing closer to the sensor," in *International Symposium on Computer Architecture (ISCA)*, 2015.
- [27] P. Esser, R. Rombach, and B. Ommer, "Taming transformers for high-resolution image synthesis," *arXiv preprint arXiv:2012.09841*, 2020.
- [28] T. Gale, E. Elsen, and S. Hooker, "The state of sparsity in deep neural networks," *arXiv preprint arXiv:1902.09574*, 2019.
- [29] G. Gao, R. Olsen, V. Sarkar, and R. Thekkath, "Collective loop fusion for array contraction," in *International Workshop on Languages and Compilers for Parallel Computing*. Springer, 1992, pp. 281–295.
- [30] M. Gao *et al.*, "Tetris: Scalable and efficient neural network acceleration with 3d memory," in *ASPLOS*, 2017, pp. 751–764.
- [31] M. Gao *et al.*, "Tangram: Optimized coarse-grained dataflow for scalable nn accelerators," in *ASPLOS*, 2019, pp. 807–820.
- [32] F.-M. Guo, S. Liu, F. S. Mungall, X. Lin, and Y. Wang, "Reweighted proximal pruning for large-scale language representation," *arXiv preprint arXiv:1909.12486*, 2019.
- [33] W.-Y. Hsiao, J.-Y. Liu, Y.-C. Yeh, and Y.-H. Yang, "Compound word transformer: Learning to compose full-song music over dynamic directed hypergraphs," *arXiv preprint arXiv:2101.02402*, 2021.
- [34] C.-Z. A. Huang, A. Vaswani, J. Uszkoreit, I. Simon, C. Hawthorne, N. Shazeer, A. M. Dai, M. D. Hoffman, M. Dinculescu, and D. Eck, "Music transformer: Generating music with long-term structure," in *International Conference on Learning Representations*, 2018.
- [35] A. Ivanov, N. Dryden, T. Ben-Nun, S. Li, and T. Hoefler, "Data movement is all you need: A case study on optimizing transformers," *arXiv e-prints*, pp. arXiv–2007, 2020.
- [36] Z. Jia, M. Zaharia, and A. Aiken, "Beyond data and model parallelism for deep neural networks," *arXiv preprint arXiv:1807.05358*, 2018.
- [37] X. Jiao, Y. Yin, L. Shang, X. Jiang, X. Chen, L. Li, F. Wang, and Q. Liu, "Tinybert: Distilling bert for natural language understanding," *arXiv preprint arXiv:1909.10351*, 2019.
- [38] N. P. Jouppi, D. H. Yoon, G. Kurian, S. Li, N. Patil, J. Laudon, C. Young, and D. Patterson, "A domain-specific supercomputer for training deep neural networks," *Communications of the ACM*, vol. 63, no. 7, pp. 67–78, 2020.
- [39] N. P. Jouppi, C. Young, N. Patil, D. Patterson, G. Agrawal, R. Bajwa, S. Bates, S. Bhatia, N. Boden, A. Borchers *et al.*, "In-datacenter performance analysis of a tensor processing unit," in *International Symposium on Computer Architecture (ISCA)*. IEEE, 2017, pp. 1–12.
- [40] S.-C. Kao and T. Krishna, "Gamma: Automating the hw mapping of

- dnn models on accelerators via genetic algorithm,” in *ICCAD*, 2020.
- [41] A. Katharopoulos, A. Vyas, N. Pappas, and F. Fleuret, “Transformers are rnns: Fast autoregressive transformers with linear attention,” in *International Conference on Machine Learning*. PMLR, 2020, pp. 5156–5165.
 - [42] K. Kennedy and K. S. McKinley, “Maximizing loop parallelism and improving data locality via loop fusion and distribution,” in *International Workshop on Languages and Compilers for Parallel Computing*. Springer, 1993, pp. 301–320.
 - [43] S. Kim, A. Gholami, Z. Yao, M. W. Mahoney, and K. Keutzer, “I-bert: Integer-only bert quantization,” *arXiv preprint arXiv:2101.01321*, 2021.
 - [44] N. Kitaev, Ł. Kaiser, and A. Levskaya, “Reformer: The efficient transformer,” *arXiv preprint arXiv:2001.04451*, 2020.
 - [45] F. Kjolstad, S. Kamil, S. Chou, D. Lugato, and S. Amarasinghe, “The tensor algebra compiler,” *Proceedings of the ACM on Programming Languages*, vol. 1, no. OOPSLA, pp. 1–29, 2017.
 - [46] H. Kwon, P. Chatarasi, M. Pellauer, A. Parashar, V. Sarkar, and T. Krishna, “Understanding reuse, performance, and hardware cost of dnn dataflow: A data-centric approach,” in *Proceedings of the 52nd Annual IEEE/ACM International Symposium on Microarchitecture*, 2019, pp. 754–768.
 - [47] H. Kwon, A. Samajdar, and T. Krishna, “Maeri: Enabling flexible dataflow mapping over dnn accelerators via reconfigurable interconnects,” *ACM SIGPLAN Notices*, vol. 53, no. 2, pp. 461–475, 2018.
 - [48] G. Lample and A. Conneau, “Cross-lingual language model pretraining,” *arXiv preprint arXiv:1901.07291*, 2019.
 - [49] H. Le, L. Vial, J. Frej, V. Segonne, M. Coavoux, B. Lecouteux, A. Allauzen, B. Crabbé, L. Besacier, and D. Schwab, “Flaubert: Unsupervised language model pre-training for french,” *arXiv preprint arXiv:1912.05372*, 2019.
 - [50] P. J. Liu, M. Saleh, E. Pot, B. Goodrich, R. Sepassi, L. Kaiser, and N. Shazeer, “Generating wikipedia by summarizing long sequences,” *arXiv preprint arXiv:1801.10198*, 2018.
 - [51] W. Lu *et al.*, “Flexflow: A flexible dataflow accelerator architecture for convolutional neural networks,” in *HPCA*. IEEE, 2017, pp. 553–564.
 - [52] A. Parashar, P. Raina, Y. S. Shao, Y.-H. Chen, V. A. Ying, A. Mukkara, R. Venkatesan, B. Khailany, S. W. Keckler, and J. Emer, “Timeloop: A systematic approach to dnn accelerator evaluation,” in *2019 IEEE International Symposium on Performance Analysis of Systems and Software (ISPASS)*. IEEE, 2019, pp. 304–315.
 - [53] N. Parmar, A. Vaswani, J. Uszkoreit, Ł. Kaiser, N. Shazeer, A. Ku, and D. Tran, “Image transformer,” *arXiv preprint arXiv:1802.05751*, 2018.
 - [54] N. Parmar, A. Vaswani, J. Uszkoreit, L. Kaiser, N. Shazeer, A. Ku, and D. Tran, “Image transformer,” in *International Conference on Machine Learning*. PMLR, 2018, pp. 4055–4064.
 - [55] J. Qiu, H. Ma, O. Levy, S. W.-t. Yih, S. Wang, and J. Tang, “Blockwise self-attention for long document understanding,” *arXiv preprint arXiv:1911.02972*, 2019.
 - [56] A. Radford, J. Wu, R. Child, D. Luan, D. Amodei, and I. Sutskever, “Language models are unsupervised multitask learners,” *OpenAI Blog*, vol. 1, no. 8, p. 9, 2019.
 - [57] J. W. Rae, A. Potapenko, S. M. Jayakumar, and T. P. Lillicrap, “Compressive transformers for long-range sequence modelling,” *arXiv preprint arXiv:1911.05507*, 2019.
 - [58] C. Raffel, N. Shazeer, A. Roberts, K. Lee, S. Narang, M. Matena, Y. Zhou, W. Li, and P. J. Liu, “Exploring the limits of transfer learning with a unified text-to-text transformer,” *arXiv preprint arXiv:1910.10683*, 2019.
 - [59] A. Roy, M. Saffar, A. Vaswani, and D. Grangier, “Efficient content-based sparse attention with routing transformers,” *Transactions of the Association for Computational Linguistics*, vol. 9, pp. 53–68, 2021.
 - [60] H. Sajjad, F. Dalvi, N. Durrani, and P. Nakov, “Poor man’s bert: Smaller and faster transformer models,” *arXiv preprint arXiv:2004.03844*, 2020.
 - [61] A. Samajdar, Y. Zhu, P. Whatmough, M. Mattina, and T. Krishna, “Scale-sim: Systolic cnn accelerator simulator,” *arXiv preprint arXiv:1811.02883*, 2018.
 - [62] V. Sanh, L. Debut, J. Chaumond, and T. Wolf, “Distilbert, a distilled version of bert: smaller, faster, cheaper and lighter,” *arXiv preprint arXiv:1910.01108*, 2019.
 - [63] Y. S. Shao *et al.*, “Simba: Scaling deep-learning inference with multi-chip-module-based architecture,” in *MICRO*, 2019, pp. 14–27.
 - [64] S. Shen, Z. Dong, J. Ye, L. Ma, Z. Yao, A. Gholami, M. W. Mahoney, and K. Keutzer, “Q-bert: Hessian based ultra low precision quantization of bert,” in *Proceedings of the AAAI Conference on Artificial Intelligence*, vol. 34, no. 05, 2020, pp. 8815–8821.
 - [65] T. Shen, T. Zhou, G. Long, J. Jiang, and C. Zhang, “Bi-directional block self-attention for fast and memory-efficient sequence modeling,” *arXiv preprint arXiv:1804.00857*, 2018.
 - [66] L. Song *et al.*, “Hypar: Towards hybrid parallelism for deep learning accelerator array,” in *HPCA*. IEEE, 2019, pp. 56–68.
 - [67] P. Sun, Y. Jiang, R. Zhang, E. Xie, J. Cao, X. Hu, T. Kong, Z. Yuan, C. Wang, and P. Luo, “Transtrack: Multiple-object tracking with transformer,” *arXiv preprint arXiv:2012.15460*, 2020.
 - [68] Z. Sun, H. Yu, X. Song, R. Liu, Y. Yang, and D. Zhou, “Mobilebert: a compact task-agnostic bert for resource-limited devices,” *arXiv preprint arXiv:2004.02984*, 2020.
 - [69] V. Sze, Y. Chen, T. Yang, and J. S. Emer, *Efficient Processing of Deep Neural Networks*, ser. Synthesis Lectures on Computer Architecture. Morgan & Claypool Publishers, 2020. [Online]. Available: <https://doi.org/10.2200/S01004ED1V01Y202004CAC050>
 - [70] Y. Tay, D. Bahri, D. Metzler, D.-C. Juan, Z. Zhao, and C. Zheng, “Synthesizer: Rethinking self-attention in transformer models,” *arXiv preprint arXiv:2005.00743*, 2020.
 - [71] Y. Tay, M. Dehghani, S. Abnar, Y. Shen, D. Bahri, P. Pham, J. Rao, L. Yang, S. Ruder, and D. Metzler, “Long range arena: A benchmark for efficient transformers,” *arXiv preprint arXiv:2011.04006*, 2020.
 - [72] N. Tesla, “V100 gpu architecture,” *Online verfügbar unter <http://images.nvidia.com/content/volta-architecture/pdf/volta-architecture-whitepaper.pdf>, zuletzt geprüft am*, vol. 21, 2018.
 - [73] A. Vaswani, N. Shazeer, N. Parmar, J. Uszkoreit, L. Jones, A. N. Gomez, Ł. Kaiser, and I. Polosukhin, “Attention is all you need,” in *Advances in neural information processing systems*, 2017, pp. 5998–6008.
 - [74] A. Vaswani, N. Shazeer, N. Parmar, J. Uszkoreit, L. Jones, A. N. Gomez, Ł. Kaiser, and I. Polosukhin, “Attention is all you need,” in *Advances in neural information processing systems*, 2017, pp. 5998–6008.
 - [75] S. Venkataramani *et al.*, “Scaleddeep: A scalable compute architecture for learning and evaluating deep networks,” in *MICRO*, 2017, pp. 13–26.
 - [76] S. Venkataramani *et al.*, “Deeptools: Compiler and execution runtime extensions for rapid ai accelerator,” *IEEE Micro*, vol. 39, no. 5, pp. 102–111, 2019.
 - [77] H. Wang, Z. Zhang, and S. Han, “Spatten: Efficient sparse attention architecture with cascade token and head pruning,” *arXiv preprint arXiv:2012.09852*, 2020.
 - [78] S. Wang, B. Li, M. Khabsa, H. Fang, and H. Ma, “Linformer: Self-attention with linear complexity,” *arXiv preprint arXiv:2006.04768*, 2020.
 - [79] W. Wang, F. Wei, L. Dong, H. Bao, N. Yang, and M. Zhou, “Minilm: Deep self-attention distillation for task-agnostic compression of pre-trained transformers,” *arXiv preprint arXiv:2002.10957*, 2020.
 - [80] Z. Wang, J. Wohlwend, and T. Lei, “Structured pruning of large language models,” *arXiv preprint arXiv:1910.04732*, 2019.
 - [81] X. Wei *et al.*, “Automated systolic array architecture synthesis for high throughput cnn inference on fpgas,” in *DAC*, 2017, pp. 1–6.
 - [82] X. Wei, Y. Liang, X. Li, C. H. Yu, P. Zhang, and J. Cong, “Tgpa: tile-grained pipeline architecture for low latency cnn inference,” in *Proceedings of the International Conference on Computer-Aided Design*, 2018, pp. 1–8.
 - [83] M. J. Wolfe, “Optimizing supercompilers for supercomputers,” Ph.D. dissertation, University of Illinois at Urbana-Champaign, 1982.

- [84] Y. N. Wu, J. S. Emer, and V. Sze, “Accelergy: An Architecture-Level Energy Estimation Methodology for Accelerator Designs,” in *IEEE/ACM International Conference On Computer Aided Design (ICCAD)*, 2019.
- [85] X. Yang *et al.*, “Interstellar: Using halide’s scheduling language to analyze dnn accelerators,” in *ASPLOS*, 2020, pp. 369–383.
- [86] A. Yazdanbakhsh, K. Seshadri, B. Akin, J. Laudon, and R. Narayanaswami, “An evaluation of edge tpu accelerators for convolutional neural networks,” *arXiv preprint arXiv:2102.10423*, 2021.
- [87] O. Zafrir, G. Boudoukh, P. Izsak, and M. Wasserblat, “Q8bert: Quantized 8bit bert,” *arXiv preprint arXiv:1910.06188*, 2019.
- [88] C. Zhang, P. Li, G. Sun, Y. Guan, B. Xiao, and J. Cong, “Optimizing fpga-based accelerator design for deep convolutional neural networks,” in *Proceedings of the 2015 ACM/SIGDA International Symposium on Field-Programmable Gate Arrays*, 2015, pp. 161–170.
- [89] W. Zhang, L. Hou, Y. Yin, L. Shang, X. Chen, X. Jiang, and Q. Liu, “Ternarybert: Distillation-aware ultra-low bit bert,” *arXiv preprint arXiv:2009.12812*, 2020.
- [90] X. Zhu, W. Su, L. Lu, B. Li, X. Wang, and J. Dai, “Deformable detr: Deformable transformers for end-to-end object detection,” *arXiv preprint arXiv:2010.04159*, 2020.